POLISH MARITIME RESEARCH 3 (119) 2023 Vol. 30; pp. 4-11
10.2478/pomr-2023-0034

INVESTIGATION OF ASYMMETRIC TWIN-RUDDER LOAD BEHAVIOUR THROUGH FREE-RUNNING MODEL TESTS

Dobrin Efremov
Evgeni Milanov
Bulgarian Ship Hydrodynamics Centre - Bulgarian Academy of Sciences, Varna, Bulgaria,

* Corresponding author: *d.efremov@bshc.bg (Dobrin Efremov)*

ABSTRACT

During tight manoeuvres, twin-screw ships equipped with two rudders located in the propeller slip stream experience a fairly large imbalance in the hydrodynamic loads on the propeller and rudders. To investigate the phenomenon of rudder asymmetric load in some depth, manoeuvring experiments based on a free-running model were set up in which the kinematics of the model, the forces on the rudder and the stock moment were recorded. In parallel, with the aim of obtaining an exact estimation of free-stream characteristics of the rudder blade, corresponding wind tunnel experiments were also performed. Based on the results of this investigation, an analysis of the interaction effects within the hull-propeller-rudder system was performed and some conclusions were drawn.

Keywords: Manoeuvrability, Twin screw–twin rudder ship, Rudder, Resistance, Rudder normal force, Interactions

LIST OF SYMBOLS

A_R	Rudder area
B	Breadth of the ship
b_R	Mean chord of the rudder blade
C_B	Block coefficient
F_N	Normal force on the rudder
F_D	Drag force on the rudder
f	Lift gradient coefficient for the rudder
h_R	Rudder height
U	Approach speed
U_R	Resultant rudder inflow velocity
u_R, v_R	Components of the rudder inflow velocity
X_R, Y_R	Surge and sway forces due to the rudder
α_R	Effective angle of inflow to the rudder
β_{R0}	Geometrical angle of inflow to the rudder
δ	Rudder angle order
δ_{N0}	Angle of the rudder at which the normal force on the rudder becomes zero

Note: Superscript symbols P, S denote port and starboard, respectively.

INTRODUCTION

Twin-screw twin-rudder propulsion and steering systems have been installed on many types of ship. In view of their very good manoeuvring performance, they are used for coastal, inland and naval vessels. Under service conditions, however, there are indications that a relatively large load imbalance can be observed between the external and internal rudders.

The asymmetry in the rudder forces on the port and starboard sides of a single-rudder manoeuvring ship is well known, and is related to the propeller slipstream twist [1]. In addition, during tight manoeuvres, the propulsion system of a twin-screw twin-rudder ship may experience significant fluctuation in the shaft loads [2,3]. Similar effects can be observed for a rudder system also, but limited investigations have been carried out [4,5].

The interactions between the hull, propeller and rudder are associated with the flow field viscosity. CFD calculations can be used to simulate the flow around rudder, including the three-dimensional separation [6]. In the case of a twin-screw twin-rudder ship, the solution becomes more difficult, due the presence of complicated interactions [7,8], and this gives rise to a need to perform experimental investigations to study this problem. There are two main goals in this case: firstly, to obtain reliable empirical results for a twin-rudder steering unit load and to analyse the asymmetry between the rudder forces during a manoeuvring motion, and secondly, to obtain data for benchmarking of the CFD results. It should be noted that the experiments reported in this paper were done with a model, meaning that the problem of scale effects of the phenomena considered here remains and will need attention in the future.

The present study focuses on EFD investigations of the forces on a twin-rudder steering system. Measurements of the rudder blade characteristics were carried out in a free stream, and were followed by free-running manoeuvring tests in which the rudder forces were recorded during both turning motion and specific tight manoeuvres. A preliminary analysis of the results and some assessments of the interaction effects are presented.

SHIP MODEL

A scale model of a fast twin-screw twin-rudder ship was used. The model was designed and produced in Bulgarian Ship Hydrodynamics Centre (BSHC). The main particulars of the hull are given in Table 1, and the body sections and a 3D view of the hull are shown in Figs. 1 and 2.

Tab. 1. Main particulars of the hull

Non-dimensional hull data	Symbol	Value
Length-to-beam ratio	L_{PP}/B	6.269
Beam-to-draft ratio	B/T	3.395
Rudder lateral area	A_R/LT	0.011
Block coefficient	C_B	0.460
Number of propellers	[–]	2
Number of rudders	[–]	2

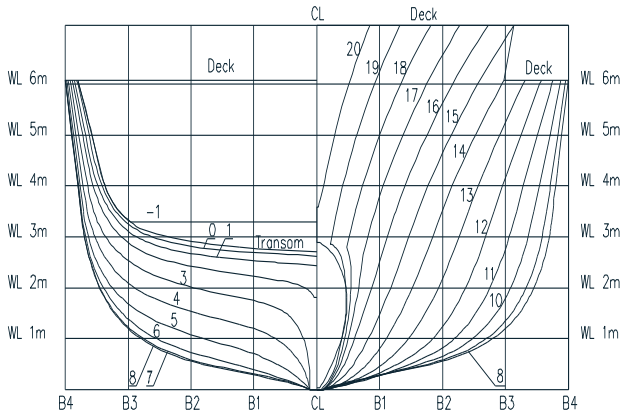

Fig. 1. View of the body sections

Fig. 2. 3D view of the hull of the model

The ship model was equipped with fixed pitch stock propellers (FPP) (Fig. 3), for which the main characteristics are shown in Table 2.

Tab. 2. Data for the propeller model

Propeller	№1	№2
Propeller diameter, mm	110.3	
Design pitch ratio at 0.7R	1.04	
Expanded blade area ratio	0.446	
Number of blades	4	
Direction of rotation	Right	Left

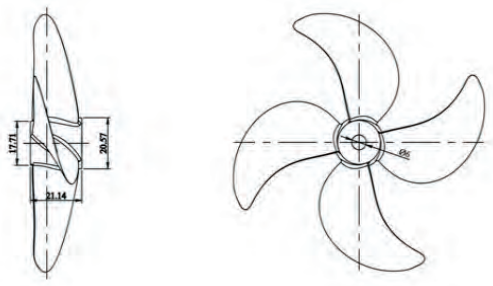

Fig. 3. View of the propeller

The model was equipped with two rudders, as summarised in Table 3. The geometry of each rudder is shown in Fig. 4. The arrangement of propellers and rudders on the model is illustrated in Fig. 5.

Tab. 3. Data for the rudder model

Characteristic	Symbol	Dimensions	Model
Rudder area	A_R	m^2	0.00545
Rudder height	h_R	m	0.1016
Rudder mean chord	b_R	m	0.0537

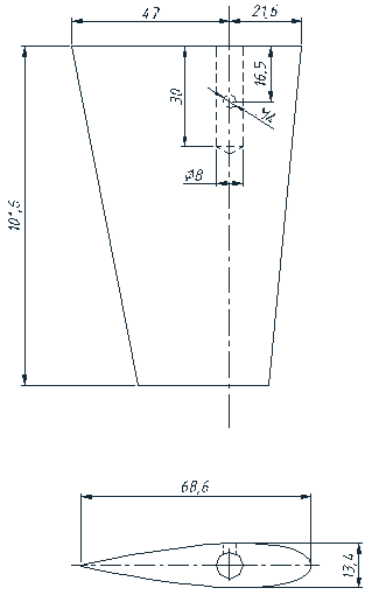

Fig. 4. Rudder geometry

Fig. 5. View showing the arrangement of rudders and propellers

FREE STREAM RUDDER CHARACTERISTICS OBTAINED VIA WIND TUNNEL EXPERIMENTS

Experimental wind tunnel setup

To obtain the free-stream rudder characteristics of the model, an experiment was carried out in the BSHC wind tunnel. The experimental model was located in the test section of the wind tunnel, labelled **1** in Fig. 6. The closed-circuit wind tunnel had an open test section of 800 × 466 mm, and was assembled from straight parts of a closed-return passage with a rectangular cross section, elbows with corner vanes, a nozzle, and an open test section (**1**). The honeycomb and two screens were placed in a closed-return passage. The rudder blade of the model (**2**) was fastened firmly via the stock (**3**) to the α mechanism (**4**), which changed the angle of attack of the rudder profile. The α mechanism was rigidly joined to the aerodynamic balance (**5**). The measurement system included the low-speed wind tunnel system and the aerodynamic balance and data processing software (based on LabVIEW and Matlab).

Fig. 6 Experimental setup in the wind tunnel (1 - Working section; 2 - Rudder blade; 3 - Rudder stock; 4 - Rotating mechanism; 5 - Six-component balance)

Results of measurements

The characteristics of the rudder blade profile are given in Fig. 7. The critical angle at which separation started was observed at an angle of attack greater than 20°. Under these conditions, the lift coefficient dropped to low values and the drag on the blade increased sharply. This region was examined using smoke visualisation, as shown in Fig. 8.

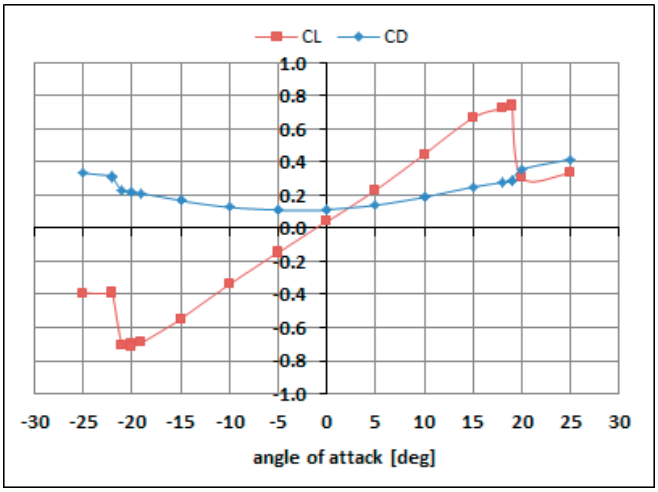

*Fig. 7. Rudder lift and drag coefficients versus angle of attack, Rn=1.93*10^5*

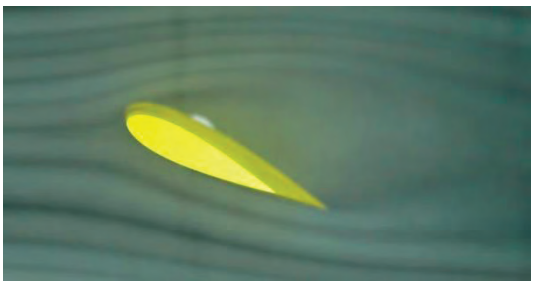

Fig. 8. Flow separation region observed with smoke visualisation

RUDDER CHARACTERISTICS FROM FREE-RUNNING MODEL TESTS

EXPERIMENTAL SETUP IN THE MANOEUVRING BASIN

Manoeuvring tests with the model were carried out in the BSHC Manoeuvring & Seakeeping Basin (Figs. 9 and 10), with main dimensions **L** × **B** × **T** = 60 × 40 × 2.5 m (maximum depth). The wave making by the model motion was damped by a wave-absorbing beach, located at the opposite side from the wave generator.

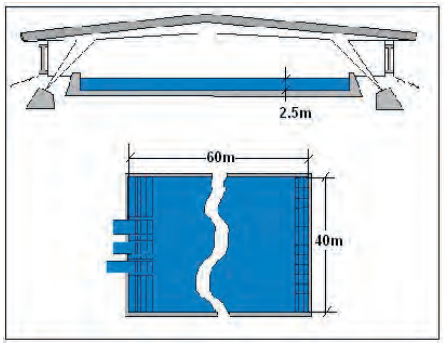

Fig. 9. Main dimensions of the manoeuvring basin

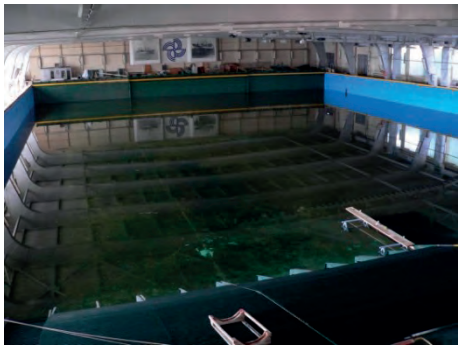

Fig. 10. The BSHC manoeuvring basin

Model equipment

The equipment needed for the free-running tests was physically divided into two types, onboard and onshore equipment, which worked together synchronised by a radio link. The onboard equipment contained all the units needed for remote control of the model and for the measurements, data acquisition and data recording, both onboard and onshore (Fig. 11).

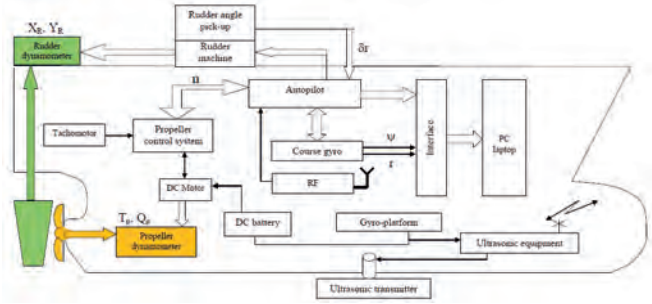

Fig. 11. Block diagram of the equipment used for the experiments

The complete model equipped for the free-running manoeuvring tests is shown in Fig. 12, and the rudder forces dynamometer is illustrated in Fig. 13.

Fig. 12. Fully equipped ship model

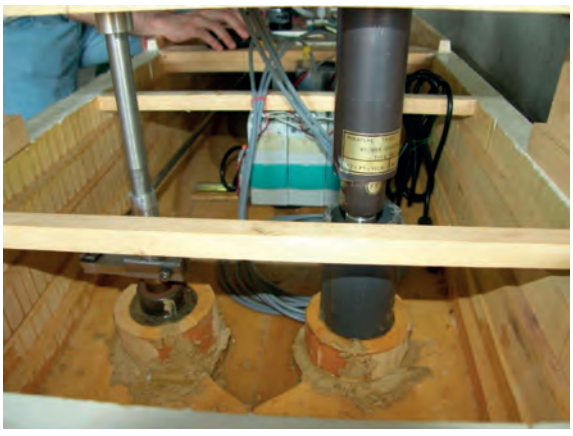

Fig. 13. Rudder force dynamometer

Experimental results and analysis

Table 4 shows a matrix of the parameters used for the experimental program. Two approach speeds were used during the free-running manoeuvring tests by varying the rudder angle. The rudder forces were originally measured in a coordinate system fixed to the rudder, and were then recalculated in a coordinate system fixed to the model. In addition to the rudder force measurements, all of the other kinematic parameters of the manoeuvring motion were recorded. During the tests, a constant RPM strategy was applied [2,9].

Tab 4. Matrix of parameters for the experiments

Manoeuvre	Initial speed [m/s]	Fn [-]	Rudder angle [deg]
Turning	1.9; 2.48	0.34; 0.44	20, 25,30,35
Williamson turn	1.9; 2.48	0.34; 0.44	$\delta = 35° \rightarrow \psi=60$/ $\delta = -35° \rightarrow \psi=180$
Steering gear test	1.9; 2.48	0.34; 0.44	35°/–35°

Time series data for the rudder resistance force F_D and the normal force F_N are given in Figs. 14–17, where the external and internal rudder (according to the direction of turning) are denoted as "ext" and "int", respectively.

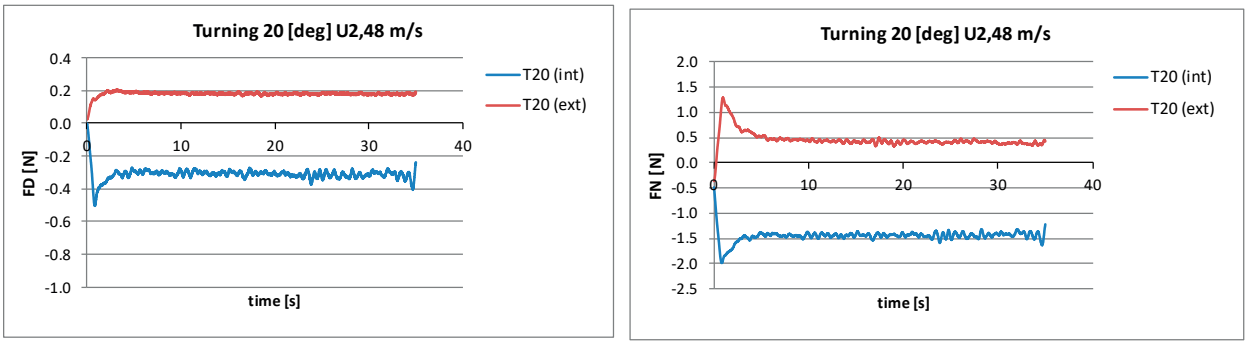

Fig. 14. Resistance F_D (left) and normal force F_N (right) for rudder turning through 20°

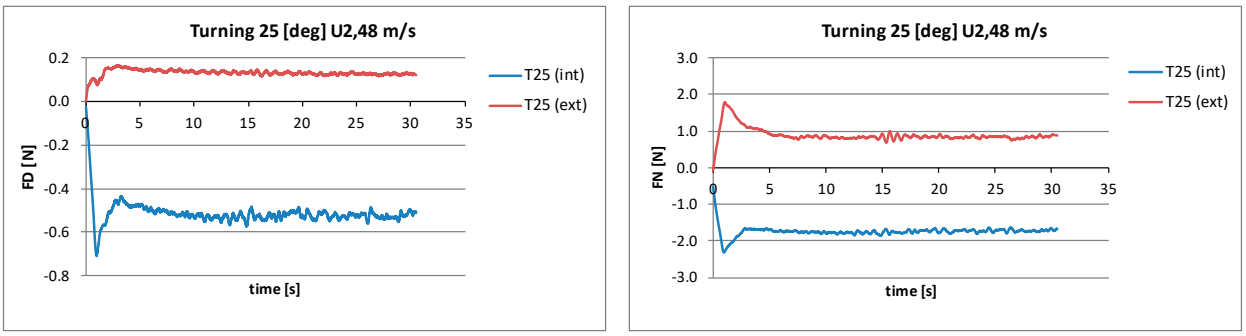

Fig. 15. Resistance F_D (left) and normal force F_N (right) for rudder turning through 25°

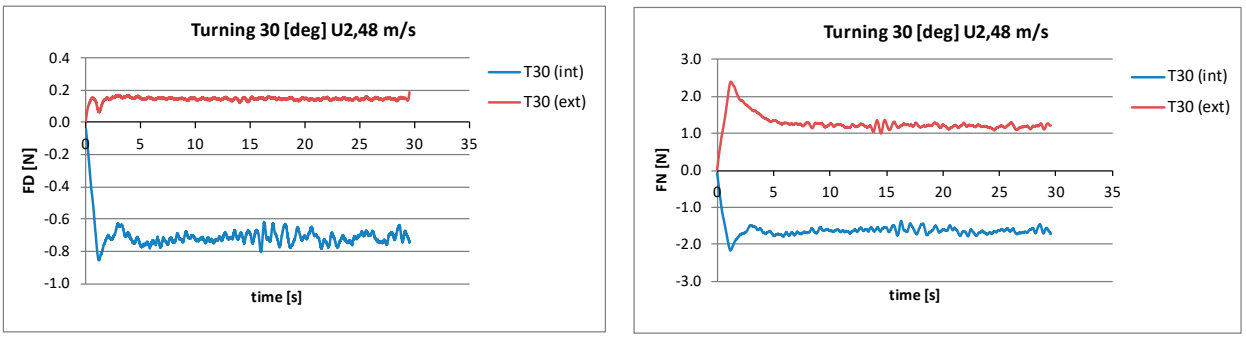

Fig. 16. Resistance F_D (left) and normal force F_N (right) for rudder turning through in 30°

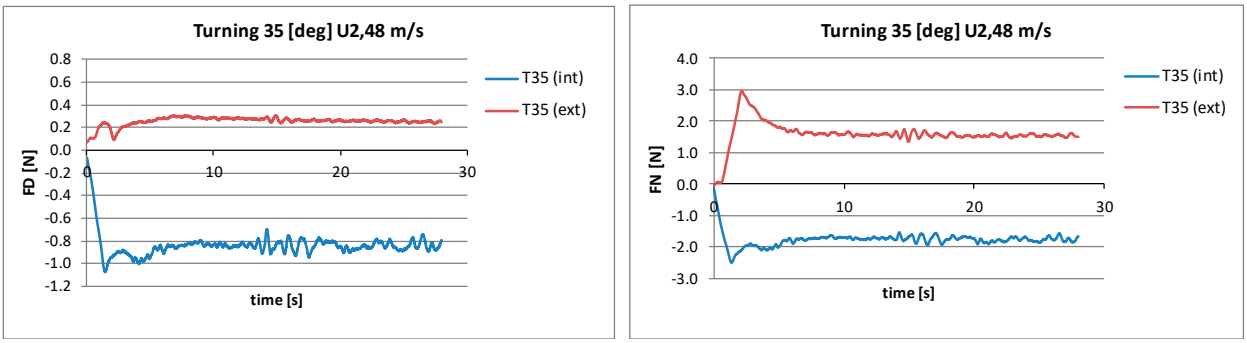

Fig. 17. Resistance F_D (left) and normal force F_N (right) for rudder turning through 35°

From the above figures, the following preliminary conclusions can be drawn. Regarding the resistance force F_D, the internal rudder load systematically increases with a characteristic peak value according the bigger rudder angle value. At the same time, the external rudder resistance increases almost monotonically. The normal rudder force F_N increases in similar way, but the difference between the two rudder loads is large. For accuracy, we note that under steady turning conditions, the periodic fluctuations in the F_D and F_N values observed after 13–15 s are likely to be due to entering of the model in the initially wave system generated by the model motion. The peak values of the rudder resistance and normal forces are illustrated in Figs. 18 and 19.

Under ship service conditions, there are two extreme manoeuvres that can take place in which the rudder system is subjected to high loads, which are known as the Williamson turn and a steering gear test. For this reason, the rudder forces were recorded as the free-running model tests were performed. Due to the specific method of rudder control in these manoeuvres, in which rudder orders are applied to both ship boards (i.e. a given rudder becomes partly external and partly internal), the measurement results are compared with time series data for a tight manoeuvre with a 35° rudder order. Fig. 20 shows a comparison of time series data for the normal rudder force recorded in a Williamson turn and in

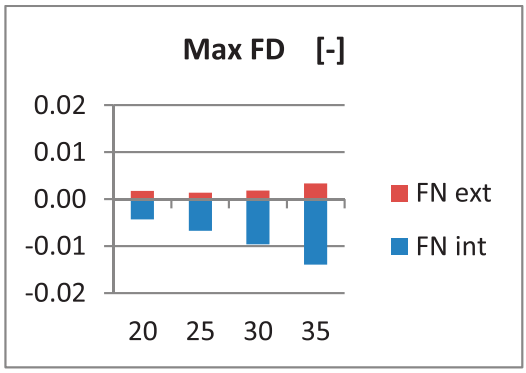

Fig. 18. Maximum values of F_D

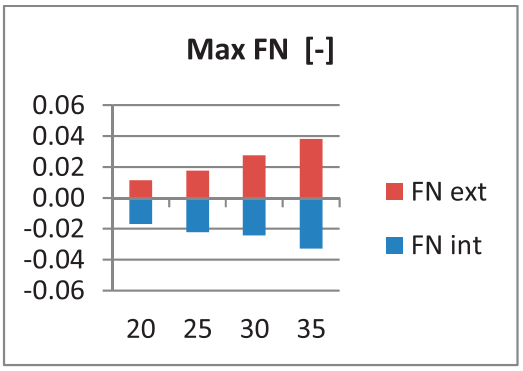

Fig. 19. Maximum values of F_N

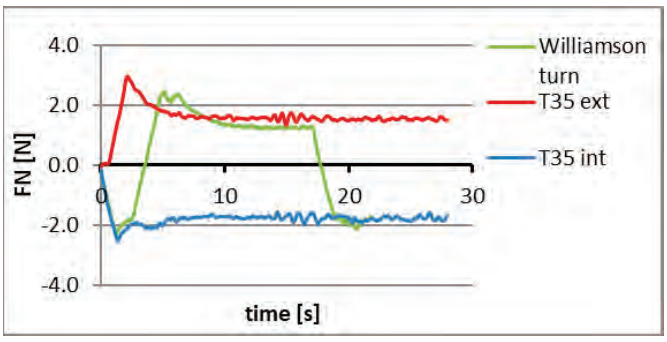

Fig. 20. F_N force over time for a Williamson turn and a 35° turning manoeuvre

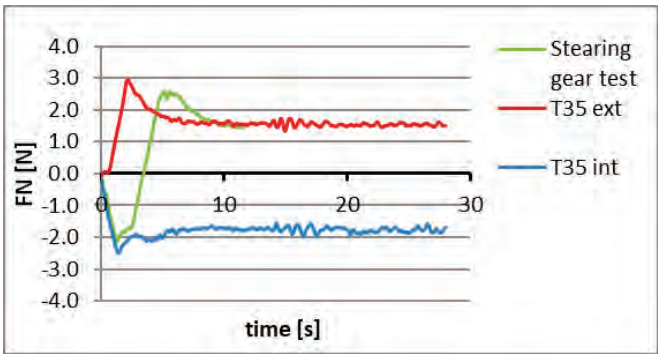

Fig. 21. F_N force over time for a steering gear test and a 35° turning manoeuvre

a 35° tight turning manoeuvre. Maximum and steady values were recorded in the latter case.
Another manoeuvre during which the maximum rudder angle needs to be applied dynamically from port to starboard and vice versa is the steering gear test, which is normally performed in a sea trial of a ship. In this manoeuvre the maximum and also the steady rudder normal force values do not exceed those in tight circulation (Fig. 21).

Estimation of interaction effects

To perform a complete analysis of the hull-propeller-rudder interactions, the results of captive model tests are needed [7]. In our case, we had data from the free-running model test, and it was therefore possible to determine reliable values for the components of the inflow velocity in the rudder region when the rudder force was equal to zero [4,5]. Following the work in [10,11], we assumed that the rudder force on the port (p) and starboard (s) rudders took the form:

$$F_N^{P,S} = 0.5\rho A_R U_R^{P,S} f_a \sin\alpha_R^{P,S} \tag{1}$$

The resultant rudder inflow velocities $U_R^{P,S}$ then have the following components:

$$U_R^{P,S} = \sqrt{u_R^{P,S\,2} + v_R^{P,S\,2}} \tag{2}$$

The effective rudder angles are:

$$\alpha_R^{P,S} = \delta + \delta_f^{P,S} - \tan^{-1}\left(\frac{v_R^{P,S}}{u_R^{P,S}}\right) \approx \delta + \delta_f^{P,S} - \frac{v_R^{P,S}}{u_R^{P,S}} \tag{3}$$

where $\delta_f^{P,S}$ is a correction to the port or starboard position in relation to the centre plane of the ship.

When the model is moving straight ahead, i.e., without drift or yaw, the lateral velocity component can be expressed as:

$$v_R^{P,S} = U\gamma_R^{P,S}\beta_{R0}^{P,S} \tag{4}$$

where $\gamma_R^{P,S}$ are the flow straightening coefficients, and $\beta_{R0}^{P,S}$ are the geometrical inflow angles for a particular rudder. If we substitute $U_R^{P,S}$ and $\alpha_R^{P,S}$ in Eq. (1) for the corresponding expressions in Eqs. (2) and (3), then in non-dimensional form we have:

$$F_N^{P,S\,\prime} = \frac{A_R}{L_{pp}T}\left(u_R^{P,S\,\prime 2} + v_R^{P,S\,\prime 2}\right) f_a \sin\left(\delta + \delta_f^{P,S} - \frac{v_R^{P,S\,\prime}}{u_R^{P,S\,\prime}}\right) \tag{5}$$

After differentiation by δ we obtain:

$$\frac{dF_N^{P,S\,\prime}}{d\delta} = \frac{A_R}{L_{pp}T}\left(u_R^{P,S\,\prime 2} + v_R^{P,S\,\prime 2}\right) f_a \cos\left(\delta + \delta_f^{P,S} - \frac{v_R^{P,S\,\prime}}{u_R^{P,S\,\prime}}\right) \tag{6}$$

By making use of the relation $\delta_{FN\,0}^{P,S} = \frac{v_R^{P,S\,\prime}}{u_R^{P,S\,\prime}}$, we can write Eq. (6) as follows:

$$\left.\frac{dF_N^{P,S\,\prime}}{d\delta}\right|_{\delta=\delta_{FNO}^{P,S}} = \frac{A_R}{L_{pp}T} u_R^{P,S\,\prime 2}\left(1+\delta_{FN0}^{P,S\,2}\right) f_a \tag{7}$$

The axial component of the rudder's inflow velocity can then be calculated:

$$u_R^{P,S\,\prime} = \sqrt{\left.\frac{dF_N^{P,S\,\prime}}{d\delta}\right|_{\delta=\delta_{FN0}^{P,S}} \frac{L_{pp}T}{A_R f_a\left(1+\delta_{FN0}^{P,S\,2}\right)}} \tag{8}$$

Based on the above expression, the lateral single rudder inflow velocities are estimated in the following way. The non-dimensional normal force for each rudder and the dimensional approach speed measured in a steady turn are given by Figs. 22 and 23, respectively.

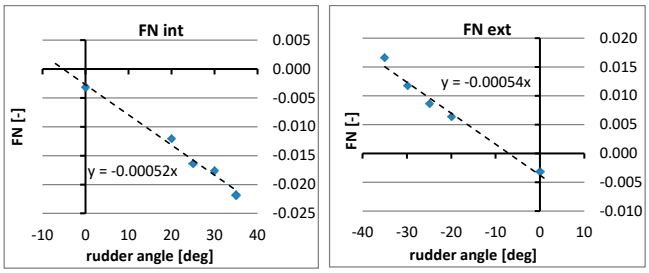

Fig. 22. Non-dimensional normal force F_N on the internal and external rudders

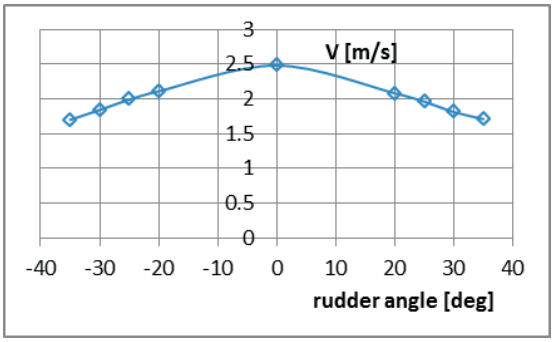

Fig. 23. Dimensional approach speed measured in a steady turn

The rudder neutral angle $\delta_{FN0}^{P\prime}$ is reached to -7.8° when rudder normal force $F_N^{P\prime}$ is equal to zero. Based on this value, the estimated rudder inflow velocity components are then as follows.

The external rudder:

$u_R^{P\prime}$ =0.94; $v_R^{P\,\prime}$ = 0.13, i.e. u_R^P = 1.99 m/s; v_R^P = 0.27 m/s.

The rudder neutral angle $\delta_{FN0}^{s'}$ is reached 5.4° when the rudder normal force $F_N^{s'}$ is equal to zero . Based on this value, the estimated rudder inflow velocity components are as follows.

The internal rudder:

$u_R^{s'}$=0.93; $v_R^{P'}$ = 0.09, i.e. u_R^P = 1.96 m/s; v_R^P = 0.19 m/s.

CONCLUSIONS AND FUTURE WORK

This paper represents an attempt to look more deeply at the characteristics of twin-rudder steering systems, with a particular focus on the asymmetry in the rudder load. The present work formed part of a BSHC project involving research in the field of hull-propeller-rudder interaction effects in the case of multi-rudder systems.

These results will form the basis for further investigations, including captive static drift model tests with the propulsion ratio and measurements of the rudder and hull forces.

ACKNOWLEDGMENTS

This work was performed as part of project financed by the Bulgarian Academy of Sciences (BAS) via grant DFNP-178/14.05.2016. The authors wish to acknowledge the BAS and BSHC staff in regard to their support for this research.

REFERENCES

1. A. Kamis, A. Fuad, A. Ashaari, C. Noor, and S. Ali, "Development of WOP mathematical model for optimum track-keeping. A ship simulation study using VLCC, focusing on hard over rudder turning circle with three stages of validation analysis," *Polish Maritime Research*, vol. 28, no. 3, pp. 156–174, 2021, eISSN 2083-7429, https://doi.org/10.2478/pomr-2021-0043.

2. A. Coraddu, G. Dubbioso, S. Mauro, and M. Viviani, "Analysis of twin screw ships' asymmetric propeller behaviour by means of free running model tests," *Ocean Engineering*, vol. 68, pp. 47–64, 2013, ISSN 0029-8018, https://doi.org/10.1016/j.oceaneng.2013.04.013.

3. G. Dubbioso and M. Viviani, "Aspects of twin screw ships semi-empirical maneuvering models," *Ocean Engineering*, vol. 48, pp. 69–80, 2012, ISSN 0029-8018, https://doi.org/10.1016/j.oceaneng.2012.03.007.

4. S. Khanfir, V. Nagarajan, K. Hasegawa, and S. K. Lee, "Estimation of mathematical model and its coefficients of ship manoeuvrability for a twin-propeller twin-rudder ship," in *Proceedings of MARSIM*, Panama City, vol. 9, pp. M159–M166, 2009.

5. S. Khanfir, K. Hasegawa, E. Kobayashi, and V. Nagarajan, "Mathematical model for manoeuvring of twin-propeller twin-rudder ship considering peculiar rudder normal force phenomenon," in *Proceedings of the International Conference on Marine Simulation and Ship Maneuverability*, Singapore, vol. 1, 2012.

6. G. Dubbioso, D. Durante, A. Di Mascio, and R. Broglia, "Turning ability analysis of a fully appended twin screw vessel by CFD. Part II: Single vs. twin rudder configuration," *Ocean Engineering*, vol. 117, pp. 259–271, ISSN 0029-8018, 2016, https://doi.org/10.1016/j.oceaneng.2016.03.001.

7. S. Khanfir et al., "Manoeuvring characteristics of twin-rudder systems: Rudder-hull interaction effect on the manoeuvrability of twin-rudder ships," Journal of Marine Science and Technology, vol. 16, no. 4, pp. 472–490, 2011, https://doi.org/10.1007/s00773-011-0140-3.

8. D. Kang, V. Nagarajan, K. Hasegawa, and M. Sano, "Mathematical model of single-propeller twin-rudder ship," *Journal of Marine Science and Technology*, vol. 13, no. 3, pp. 207–222, 2008, https://doi.org/10.1007/s00773-008-0027-0.

9. G. Dubbioso and M. Viviani, "Experimental investigation of asymmetrical propeller behavior of twin screw ships during manoeuvers," in *Proceedings of the International Conference on Marine Simulation and Ship Maneuverability*, Singapore, vol. 1, 2012.

10. H. Yasukawa and Y. Yoshimura, "Introduction of MMG standard method for ship maneuvering predictions," *Journal of Marine Science and Technology*, vol. 20, no. 1, pp. 37–52, 2015, https://doi.org/10.1007/s00773-014-0293-y.

11. Y. Yoshimura, "Mathematical model for manoeuvring ship motion (MMG model)," in *Workshop on Mathematical Models for Operations Involving Ship-Ship Interaction*, Tokyo, pp. 1-6, August, 2005.